

**Task 2b Final Report  
Windborne Debris Study  
Contract Number 12-00005-00**

Presented to the

Florida Building Commission  
State of Florida Department of Business and Professional Regulation

by

Forrest J. Masters, Ph.D., P.E., masters@ce.ufl.edu, (352) 392-9537 x 1505  
Kurtis R. Gurley, Ph.D., kgurl@ce.ufl.edu, (352) 392-9537 x 1508  
David O. Prevatt, Ph.D., P.E. (MA), dprev@ce.ufl.edu, (352) 392-9537 x 1498

Graduate Students:

Craig R. Dixon  
Daniel J. Smith

Engineering School for Sustainable Infrastructure & Environment  
University of Florida

June 15, 2013

## Table of Contents

1. Deliverables.....	1
2. Summary of Activities for Task 2(b).....	1
2.1. Review of Research Findings.....	<b>Error! Bookmark not defined.</b>
2.2. Executive Summary.....	<b>Error! Bookmark not defined.</b>
3. Background Information.....	2
3.1. Supporting Research.....	2
3.2. Requirements of FBC Building Section 1609.5.3.....	4
3.3. Requirements of FBC Building Section 1716.2.....	4
4. Project Overview.....	4
4.1. ERP 1: Characterize Wind Loads on Field Tile.....	4
4.2. ERP 2: Direct Load Measurement at Field Tile Fastening.....	5
4.3. ERP 3: Fastening Load Resistance Testing.....	5
4.4. ERP 4: Wind Loads on Hip and Ridge Tiles.....	5
5. Research Components.....	5
5.1. Wind Pressure Distributions on Field Roofing Tiles.....	5
5.1.1. Model Roofing Tiles.....	6
5.1.2. Testing Apparatus.....	7
5.1.3. Pressure Scanning System.....	7
5.1.4. Velocity Measurement System.....	8
5.1.5. Test Deck Preparation.....	8
5.1.6. Test Specimen Preparation.....	8
5.1.7. Results: Approach Flow Fields.....	11
5.1.8. Results: Surface Pressure Distribution.....	14
5.2. Attachment Forces Restraining Field Roofing Tiles.....	16
5.2.1. Experimental Configuration.....	16
5.2.2. Testing Apparatus.....	17
5.2.3. Load Cell Measurement System.....	17
5.2.4. Velocity Measurement System.....	17
5.2.5. Test Deck Preparation.....	18
5.2.6. Instrumented Roofing Tiles.....	18
5.2.7. Results.....	19
5.3. Mechanical Resistance of Roof Attachments.....	21
5.3.1. Experimental Configuration.....	21
5.3.2. Testing Apparatus.....	22
5.3.3. Specimen Preparation.....	22
5.3.4. Experimental Procedure.....	23
5.3.5. Results.....	23
5.3.6. Conclusions.....	25
5.4. Wind Loading of Hip and Ridge Tiles.....	27
5.4.1. Testing Apparatus.....	27
5.4.2. Test Building.....	28
5.4.3. Instrumentation.....	28
5.4.4. Testing Procedure.....	29
5.4.5. Preliminary Results.....	31

5.4.6. Conclusions .....34

## List of Figures

Figure 1. Inside view of model roofing tile. Medium profile tile shown. ....	6
Figure 2. View of low-, medium- and high-profile model roofing tiles (shown left to right) .....	7
Figure 3. Schematic of the Dynamic Flow Simulator (DFS) .....	7
Figure 4. Turntable configuration used in Phase I testing.....	9
Figure 5. Mechanically fastened high profile model in Phase I configuration (45° wind angle)..	10
Figure 6. Foam adhesive set medium profile array studied in Phase II .....	11
Figure 7. The approach wind velocity field normalized by reference velocity for the isolated tile .....	12
Figure 8. Cobra probe rake positioned above the medium profile roofing tile array .....	13
Figure 9. High, medium, and low profile tile approach wind velocity fields normalized by reference velocity .....	13
Figure 10. Upper surface, lower surface, and net spatial $C_p$ distributions for high profile tile array with mechanical direct to deck installation .....	14
Figure 11. Comparison of lift coefficient values to specified values in the Florida Building Code .....	16
Figure 12. Six-axis load cell and measured forces/moments .....	17
Figure 13. Side view of the load cell arrangement.....	18
Figure 14. Medium profile load cell arrangement.....	18
Figure 15. Measured attachment forces (left pane) and moments (right pane) for the low profile roofing tile as a function of wind speed .....	19
Figure 16. Measured attachment forces (left pane) and moments (right pane) for the medium-profile roofing tile with battens as a function of wind speed .....	20
Figure 17. Measured attachment forces (left panes) and moments (right panes) for the high-profile roofing tile installed with battens (upper panes) and direct to deck (lower panes) as a function of wind speed .....	21
Figure 18. Mechanical uplift testing apparatus and testing arrangement.....	22
Figure 19. Moment-load diagrams for low- and medium-profile roofing tiles.....	26
Figure 20. Florida International University Wall of Wind subsonic wind tunnel testing facility.	27
Figure 21. Test building (a) elevation plan and (b) as-built. ....	28
Figure 22. Roof plan with instrumented tiles on edge (T), ridge (R), and hip (H) roof conditions .....	29
Figure 23. Hip and ridge tile (a) dimensions and location of top surface static pressure taps on (b) hip and (c) ridge tiles .....	29
Figure 24. Wind directions .....	30
Figure 25. Contour plot of hip tile R2's mean external pressure coefficient normalized to mean approach flow conditions at mean roof height. The blue dots represent the location of surface pressure measurement. ....	32
Figure 26. Contour plot of ridge tile R8's mean external pressure coefficient normalized to mean approach flow conditions at mean roof height. The blue dots represent the location of surface pressure measurement. ....	32
Figure 27. Hip tile lift coefficients referenced to the mean approach flow measured at mean roof height vs. wind direction. ....	33
Figure 28. Ridge tile lift coefficients referenced to the mean approach flow measured at mean roof height vs. wind direction.....	33



## List of Tables

Table 1. Phase I test matrix variables .....	9
Table 2. Phase II test matrix variables.....	10
Table 3. Test matrix variables .....	16
Table 4. Six-axis load cell sensing ranges and resolutions .....	17
Table 5. Test Matrix Variables.....	22
Table 6. Attachment Resistance Expressed as a Moment - $M_f$ (ft-lbf).....	25
Table 7. Test matrix variables .....	27
Table 8. Test number, wind direction, and corresponding mean approach wind speed.....	30

## Final Report for 2012-13 Scope of Work

### 1. Deliverables

Investigate the susceptibility of shingle and tile roof systems to failure in high winds. The contractor is authorized to spend up to \$135,121 on Tasks 2(a) and 2(b).

(a) Asphalt Shingle Roof Systems. The Contractor will continue research initiated for the project entitled, “Residential Roof Covering Investigation of Wind Resistance of Asphalt Shingles” sponsored by the Southeast Region Research Initiative (SERRI) through Oak Ridge National Laboratory. The Contractor shall submit the final SERRI report (due in Fall 2012) plus any supplemental information about project activities occurring beyond that time.

**(b) Roof Tile Systems. The Contractor will perform research on the wind loading of hip and ridge tile attachments. The findings will supplement research conducted during 2011-2012 directed at the installation of field roof tiles on low-rise buildings located in high wind areas (see Task 3 in the 2011-2012 scope of work). The Contractor will coordinate with roofing experts (e.g., Roofing Tile Institute) to develop a report for distribution. The contractor shall provide an interim progress report and an ending report on this task.**

Support provided for (a) and (b) may be used as matching funds for future grant proposals investigating the performance of discontinuous roof systems.

Note: A summary of activities for Task 2(a) was provided in a separate report

### 2. Summary of Activities for Task 2(b)

Findings in this report should be considered preliminary until the oversight committee has reviewed its contents. The report will be distributed to the Roofing Tile Institute, the Insurance Institute for Business and Home Safety, and companies that make or install roofing tile products before the end of the performance period to get feedback. These groups have already provided initial feedback on the development of research plans discussed herein.

A series of four experiments were conducted to investigate the wind resistance of roofing tile systems and evaluate *2010 FBC Florida Building Code* provisions with regard to roofing tile system design. The key findings and implications to code provisions for each experiment are summarized in this section.

The objective of the first experiment was to characterize the wind-induced surface pressures on roofing tiles for variety of different wind speeds and attachment configurations. This experiment was used to directly evaluate the methodology presented by *TAS 108-95 Test Procedure for Wind Tunnel Testing of Air Permeable, Rigid, Discontinuous Roof Systems*. The results of *TAS 108-95* are used directly to calculate design loads for roofing tiles. Key findings are that *TAS 108-95* adequately estimates the wind-induced lifting forces on roofing tiles for wind angle of attack perpendicular to the leading edge (i.e., head-on), however *TAS 108-95* does not require testing for multiple wind angles of attack. There is an absence of prescribed dimensions for the wind tunnel testing apparatus required by *TAS 108-95*. Wind tunnel dimensions may significantly alter experimental results and increase the difficulty associated with replicating testing procedures.

The second experiment was conducted as a validation step for the first. The objective was

to directly measure the forces at attachment locations of roofing tiles specimens. Measured attachment forces were compared to predicted attachment loads produced by the first experiment. A key finding was that withdrawal loads on mechanically attached roofing tiles may increase significantly with deflection of the tile leading edge. The findings of this experiment may offer insight regarding the failure mechanism of mechanically attached roof tiles subjected to wind load. Furthermore, increased understanding of wind loads on roofing tiles experiencing tail deflection due to wind uplift may have implications for the attachment resistance testing method presented by *TAS 102-95 Testing Procedure for Static Uplift Resistance of Mechanically Attached, Rigid Roof System*.

The objective of the third experiment was to measure the attachment resistance of mechanically attached roofing tile specimens. This experiment is used to directly evaluate the methodology presented by *TAS 102-95*. Key findings are a lack of clarity in several areas of *TAS 102-95* methodology. There is an absence of prescribed fastener installation depth through installation holes. Variability in fastener depth may significantly affect resistance values. In addition, the angle of load application prescribed by *TAS 108-95* may not be representative of the orientation of wind loads on roof tiles.

The objective of the fourth experiment was to measure surface pressures on the upper and lower surfaces of hip and ridge tiles when immersed in wind from varying direction. Key findings indicate that the highest wind load on hip and ridge tiles occur for wind flow directed parallel to the leading edge for hip and ridge tile. Additional research is necessary to evaluate the failure modes of hip and ridge tiles. The *2010 Florida Building Code* references *FRSA/TRI 07320* for design of hip and ridge tiles. Design values are presented in *FRSA/TRI 07320* but details regarding the methodology are absent.

### **3. Background Information**

The purpose of this section is to summarize the wind design methodology for air permeable rigid roofing tiles prescribed by the *2010 Florida Building Code*. The supporting research behind the design approach is reviewed first, followed by the specific guidelines in the *2010 Florida Building Code*.

#### **3.1. Supporting Research**

The wind design procedures for air permeable rigid roofing tiles in the *2010 Florida Building Code* originate from Redland Technology's 1991 report *Fixing Studies for MRTI Normal Weight Tiles – SBCCI Submissions* (henceforth, Redland Report). The report describes a design methodology to calculate the wind loads acting on roofing tiles and the resistance of the tile to wind uplift for various tile attachment methods (e.g., fasteners or clips). Two experiments were performed by Redland Technology to develop their design method:

- 1) Wind loads were estimated from wind tunnel tests where surface pressures on medium and high profile roofing tiles were measured as wind was blown across the tile located in a sample tile array.
- 2) Wind uplift resistance was estimated from constant displacement (e.g., static) uplift tests that quantified the uplift resistance of roofing tiles with various attachment methods.

In the first experiment, wind-induced surface pressures were measured on four tile configurations: (1) medium profile tile without battens, (2) medium profile tile with battens, (3) medium profile tile without battens with a 50.8 mm (2 in) tail lift, and (4) high profile tile without battens. For each configuration, an array of tiles was installed on a 1.5 m (4.9 ft) wide by 3.5 m (11.5 ft) long deck and placed in a 1 m (3.3 ft) high by 1.5 m (4.9 ft) wide open circuit wind tunnel. The arrays were oriented such that the leading edge of each tile was perpendicular to the wind flow. For each array, one tile located 2.5 m (8.2 ft) from the windward edge and in the centermost width of the array was used for top and bottom surface pressure measurement at twenty locations along the centerline of the tile, parallel to the direction of wind flow.

Wind was blown across the deck in a 4.5 m/s (10 mph) step and 60-second hold pattern starting at 31 m/s (70 mph) and ending at 125 mph (58 m/s). Turbulence characteristics of the approach wind and the vertical profile of the wind from the tile's surface upwards were not reported. Mean wind velocity and static pressure in the free-stream were measured, however, using a pitot-static tube placed 100 mm (4 in) above the surface of the tile deck and 1.5 m (4.9 ft) upwind of the instrumented tile. The following data were recorded for each hold period: mean static pressure of each tile tap, mean wind velocity, and mean static pressure measured by the pitot-static tube.

All tap measurements were transformed into a dimensionless pressure coefficients ( $C_{pi}$ ) referenced to the static and velocity pressure measurements made 100 mm (3.9 in) above the tile deck. Each tap was associated with a tributary area on the tile corresponding to the tile's width by one-half the distance from each of the two adjacent taps. Redland assumed that the pressures along the width of each tributary strip were equivalent, despite the varying cross-section of the high and medium profile tiles (i.e., not a flat plate). Using the pressure coefficients and corresponding tributary area, a coefficient of lift ( $C_L$ ) was then calculated to represent a dimensionless average net force acting to lift the roofing tile (Eq. 1). A coefficient of moment ( $C_{Ma}$ ) was also computed, representing dimensionless moment acting about the axis of rotating near the head of the tile (Eq. 2).

$$C_L = \frac{\sum C_{pb} \delta_b}{l * b} - \frac{\sum C_{tb} \delta_t}{l * b} \quad (1)$$

$$C_{Ma} = \frac{\sum C_{pb} \delta_b l'_b}{l^2 * b} - \frac{\sum C_{tb} \delta_t l'_t}{l^2 * b} \quad (2)$$

where  $C_{pb}$  = pressure coefficient on the bottom surface of the tile,  $\delta_b$  = tributary area of corresponding bottom surface pressure coefficient,  $C_{pt}$  = pressure coefficient on the top surface of the tile,  $\delta_t$  = tributary area of corresponding top surface pressure coefficient,  $l$  = length of the tile,  $l'_b$  = moment arm acting at each pressure tap (bottom surface),  $l'_t$  = moment arm acting at each pressure tap (top surface), and  $b$  = exposed width of the tile.

The coefficients of lift and moment are referenced to the near-roof velocity and static pressure. However, for design by building codes it is required that those coefficients be referenced to the approach velocity and static pressure. To accomplish this reference transformation, Redland Technology employed Bernoulli's equation, equating the total pressure in the approach flow to the total pressure in the near-roof flow using the static and velocity pressure for each flow location (Eq. 3). The equation is valid for roof locations outside of flow-separated regions where the flow is inviscid and irrotational. Neither condition is valid for flow

near the roof, but this approach does provide a reasonable first approximation to calculate the speed-up over the roof. The relationship is convenient because ASCE 7 external pressure coefficients are reference to approach wind flow. External pressure coefficients are employed in this calculation as proxy for the static pressure measured by the pitot-static tube in the wind tunnel tests of the roofing tiles.

$$P_{sa} + \frac{1}{2}\rho V_a^2 = P_{sr} + \frac{1}{2}\rho V_r^2 \quad (3)$$

where  $P_{sa}$  = approach wind static pressure,  $\rho$  = air density,  $V_a$  = approach wind velocity,  $P_{sr}$  = near-roof static pressure, and  $V_r$  = near-roof wind velocity. The resulting equation of this energy balance (Eq. 4) is used in Equation 16-33 in the *2010 Florida Building Code*.

$$q_r = q_a (1 - C_p) \quad (4)$$

where  $q_r = \frac{1}{2}\rho V_r^2$  = near-roof wind velocity pressure,  $q_a = \frac{1}{2}\rho V_a^2$  = approach wind velocity pressure,  $C_p$  = external pressure coefficient referenced to approach wind conditions (e.g., ASCE 7-10 components and cladding external pressure coefficients).

### 3.2. Requirements of FBC Building Section 1609.5.3

Wind loads on structural components are covered in Section 1609 of the *2010 Florida Building Code – Building Chapter*. Per Section 1609.5.2, rigid tile roof coverings that are air permeable and installed over structural roof decking are permitted to be designed for wind resistance by Section 1609.5.3.

Wind loads on rigid tile roofing are determined in Section 1609.5.3 by Equation 16-33 (Eq. 1 below) that equates the wind-induced uplift moment acting on an individual tile ( $M_a$ ) to the product of the wind velocity pressure ( $q_h$ ), lift coefficient ( $C_L$ ), exposed width of the tile ( $b$ ), length of the tile ( $L$ ), moment arm ( $L_A$ ), and unity minus the external roof pressure coefficient for each applicable roof zone ( $GC_p$ ).

$$M_a = q_h C_L b L L_A [1.0 - GC_p] \quad (5)$$

### 3.3. Requirements of FBC Building Section 1716.2

The experiment in Section 1716.2 is Testing Application Standard 108-95 and consists of measurements of surface pressures on roofing tiles in a wind tunnel as wind is blown across the roof deck. Wind speeds in the test section follow a step-and-hold pattern, ranging from 70 mph to 110 mph at 10 mph step increments. The test section measures four or more laid components wide by nine or more courses flow-wise with an instrumented tile located approximately seven courses from the most-upwind course in the center of the test section's width.

## 4. Project Overview

Four experimental research plans (ERP) were carried out to study wind load effects on roofing tile systems. The objectives of each experiment and the directive for evaluating 2010 FBC roofing tile system design methodology are included in the following sections.

### 4.1. ERP 1: Wind Pressure Distributions on Field Roofing Tiles

The research objectives of this experiment are to: [1] characterize the wind pressure distribution

on low-, medium-, and high- profile field tiles and [2] resolve the resultant load path and intensity through the tile attachments (e.g., mechanical fasteners, foam). The results of this experiment are used to evaluate the methodology for measuring wind loads on roof tiles presented by *TAS 108-95 - Test Procedure for Wind Tunnel Testing of Air Permeable, Rigid, Discontinuous Roof Systems*. Calculated wind load parameters are also compared to product approval values.

#### **4.2. ERP 2: Direct Load Measurement at Field Tile Fastening**

The research objectives of this experiment were to: [1] directly quantify the reaction forces of field tile attachments and [2] compare these results to the reaction forces derived from pressure distributions obtained during ERP 1. Directly measuring forces at the tile attachments within an array incorporates the loading contributions of the tile system surrounding the specimen tile. The analysis presented in ERP 1 and TAS 108-95 does not consider this interaction. Measured forces and moments at the tile fastening location are used to evaluate the effectiveness of wind loads predicted by analysis during ERP 1. Results were used in conjunction with ERP 1 findings to evaluate the effectiveness of TAS 108-95.

#### **4.3. ERP 3: Fastening Load Resistance Testing**

The research objectives were to: [1] quantify the mechanical uplift resistance of standard field tile attachment configurations and [2] compare measured attachment resistances to the wind-induced reaction forces obtained theoretically and experimentally during ERP 1 and 2, respectively. In addition, results of this experiment are used to assess the methodology presented by TAS 102-95 for calculating the attachment resistance of mechanically attached roofing tiles. Resultant attachment resistances will also be compared to product approval values.

#### **4.4. ERP 4: Wind Loads on Hip and Ridge Tiles**

The research objectives are to: [1] characterize the wind induced surface pressures acting on hip and ridge tiles installed on a high profile tile roof and loaded via boundary layer flow [2] resolve the resultant load path and intensity through the tile attachments. Results will be discussed along with requirements for hip and ridge tiles as specified by FRSA/TRI 07320.

These experimental research plans are summarized below topically.

### **5. Research Components**

#### **5.1. Wind Pressure Distributions on Field Roofing Tiles**

The University of Florida Dynamic Flow Simulator (DFS) was used to generate near roof wind load conditions across an isolated model tile (Phase I) and a model tile installed within a partial mockup of a tile roof system (Phase II). Specimens were installed on an interchangeable roof deck mockup that attaches to the bottom of the high speed test section of the DFS. To characterize wind loading, full-size model replicas of low-, medium- and high- profile tiles (henceforth referred to as “model tiles”) were used to measure pressures on the tile surfaces through 256 pressure taps that connect to a pressure scanning system. Three-axis wind velocities were measured with Turbulent Flow Instruments Cobra Probes mounted to the mockup roof deck. The experiment was divided into two testing phases. The objective of Phase I was to characterize the wind pressure distribution on a single field tile. The objective of Phase II was to

characterize the wind pressure distribution on a field tile installed within a tile array. Specimens for each phase were subjected to wind load inside the DFS test section and pressures on the surfaces of the model tiles were captured.

**5.1.1. Model Roofing Tiles**

Replicas of low-, medium-, and high- profile roofing tiles approved for use in the state of Florida were rapid prototyped at the wind tunnel facility at the University of Western Ontario. Hollow shells of the tiles were fabricated from resin impregnated with vinyl tubes at each pressure measurement location (See Figures 1 and 2). Each model has 256 pressure taps distributed throughout its upper, lower, and leading edge surfaces. Each tap connects to a 1.6 mm (0.063 in) diameter vinyl tube inside of the model. Tubes exit the model through the surface of the trailing edge and connect to respective ports on a pneumatic bulkhead connector. All tubes are 173 cm (68 in) so as to achieve consistent tubing dynamic response characteristics.

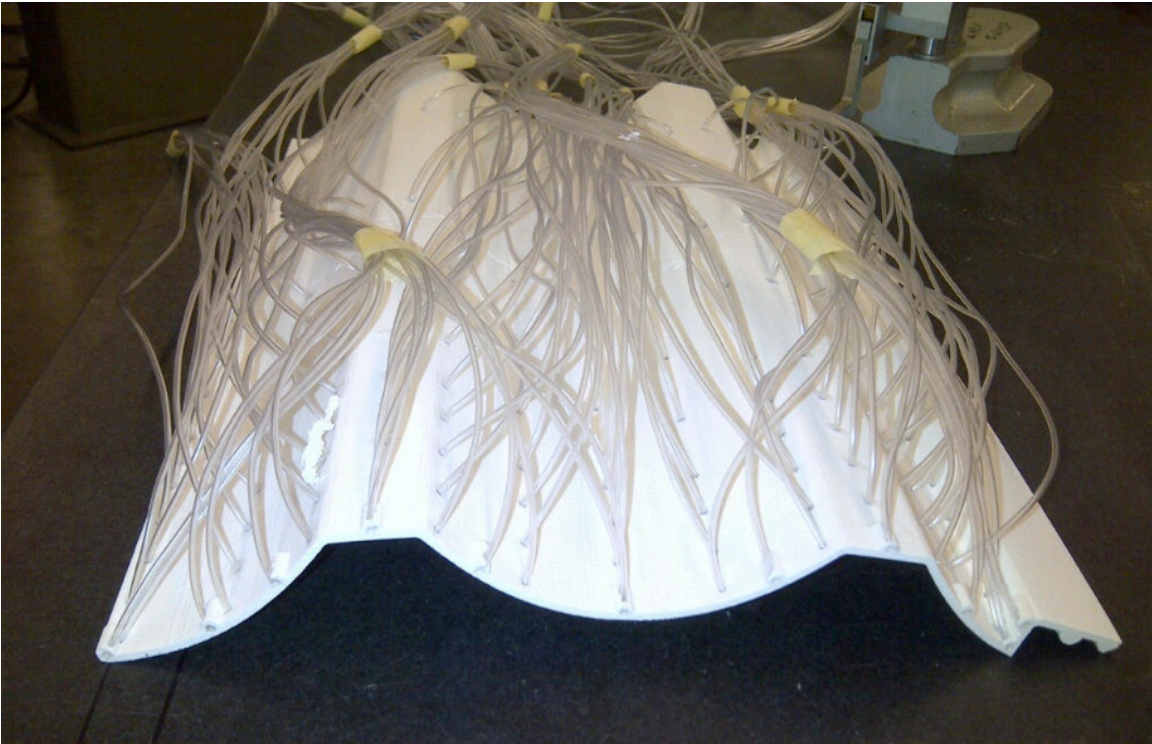


Figure 1. Inside view of model roofing tile. Medium profile tile shown.



Figure 2. View of low-, medium- and high-profile model roofing tiles (shown left to right)

### 5.1.2. Testing Apparatus

The Dynamic Flow Simulator (DFS) was used to generate wind above the test deck (Figure 3). Air enters the DFS through a 1.52 m (5 ft) diameter inlet and passes through an actively controlled opposed-blade damper system, which can oscillate at up to a 10 Hz. The air is then pulled through an 1800 HP centrifugal blower that connects to a settling chamber consisting of a wide angle diffuser turbulence screens, a honeycomb, and a 5:1 ratio contraction duct that connects to the test section. The cross sectional area at the entrance to test section is 213 cm (7 ft) wide by 38 cm (1.25 ft) tall. At the exit, the width is 213 cm (7 ft); however, the height may be adjusted to regain static pressure lost due to friction across the test section. The test decks were attached to the 243 cm (8 ft) long by 182 cm (6 ft) wide opening in the bottom floor of the test section using a pneumatic lift located below the test section. The top surface of the test deck sits at the same horizontal plane as the bottom floor of the test section.

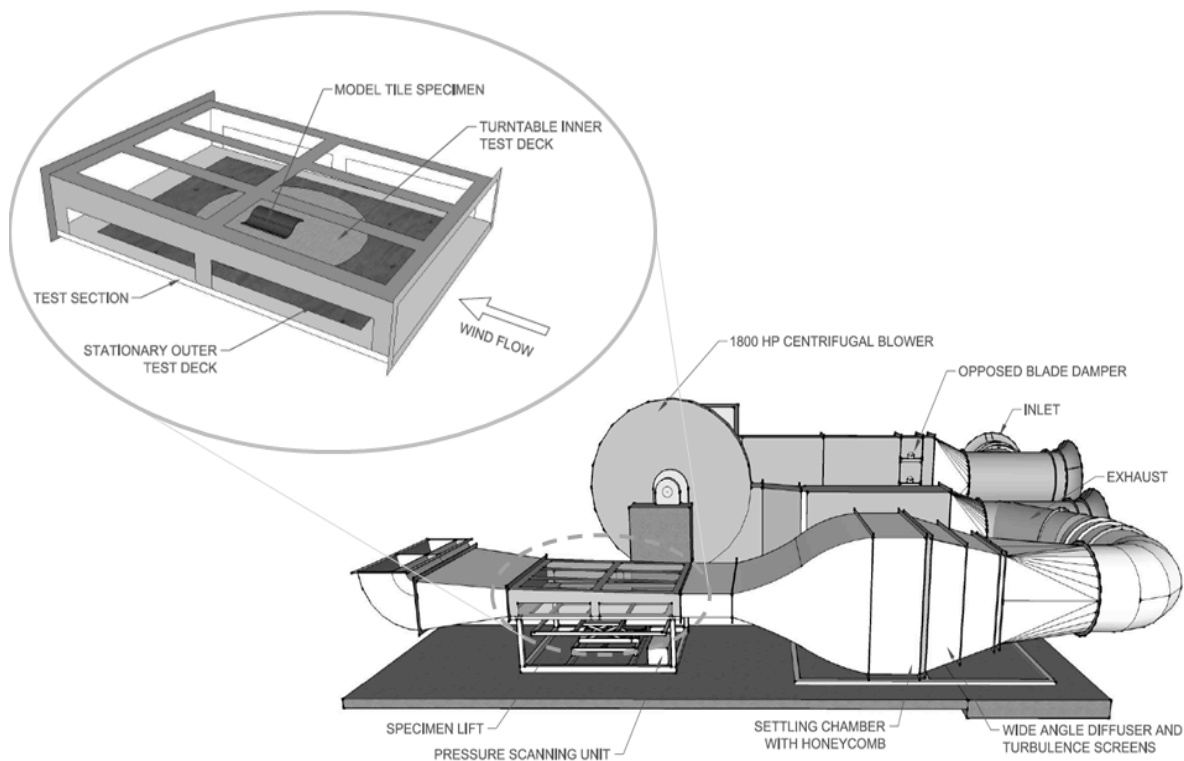


Figure 3. Schematic of the Dynamic Flow Simulator (DFS)

### 5.1.3. Pressure Scanning System

Each tile model has 256 pressure port outputs that connect to a Scanivalve Corporation pressure scanning system (PSS) capable of 625 Hz sampling rate. The system consists of four zero, operate, and calibrate (ZOC33) electronic pressure scanning modules, one single processing device called the Ethernet Remote A/D (ERAD), a power supply, and a chassis that holds the hardware. Each ZOC33 module incorporates 64 individual silicon pressure transducers calibrated to a maximum range of  $\pm 5$  in water column ( $\pm 1245$  Pa), a high speed multiplexer (45 kHz), and

an instrumentation amplifier. The ZOC33 modules also have a calibration valve that allows sensors to be automatically calibrated and input lines to be purged of contaminants or condensation. All four ZOC33 modules connect to the ERAD. The ERAD converts analog signal outputs from the ZOC33 modules into digital signals through a programmable digital signal processor (DSP). The DSP performs high speed conversion functions on the digital signals and outputs engineering units of pressure via Ethernet TCP/IP. The DSP also utilizes a pressure temperature look-up table to compensate the pressure sensors for temperature changes, thus reducing thermal errors. A network attached storage (NAS) device is used to store raw data streaming from the ERAD via Ethernet TCP/IP.

#### **5.1.4. Velocity Measurement System**

Turbulent Flow Instrument Cobra Probes (henceforth “Cobra Probes”) are multi-hole pressure probes able to resolve the 3-components of velocity and local static pressure. Cobra Probes were used to measure three-axis wind velocities inside the test chamber. Characteristics of the probes include an ability to measure flow within a +/- 45° cone, a maximum sampling frequency of 2000 Hz, accuracy of better than +/- 0.5 m/s and +/- 1° yaw up to 30% turbulence intensity. Cobra probe reference locations are detailed in Section 2.4.1.10.

#### **5.1.5. Test Deck Preparation**

Six test decks were constructed. The dimensions of each test deck were 241 cm (95 in) by 180 cm (71 in), allowing 1.25 cm (0.5 in) clearance on all sides for attachment to the 183 cm (6 ft) x 244 cm (8 ft) DFS test section opening. Each test deck consists of 2 x 6 framing at 61 cm (2 ft) on center with additional 2x6 framing at either end. All framing connections were completed using #8 x 2.5 in galvanized screws. Two saw-cut sheets of 122 cm (4 ft) by 183 cm (6 ft) plywood were fastened to the test deck framing using #8 x 2.5 in galvanized screws at 15 cm (6 in) on center. One test deck also included a 66 cm (26 in) diameter turntable for Phase I testing. Test deck sheathing consisted of 15/32 performance category APA rated plywood with 32/16 span rating, exposure 1 bond classification, and 0.451 in (11.455 mm) thickness. A self-adhered underlayment produced by Eagle Roofing and approved for use with roof tile systems, was installed on each test deck.

#### **5.1.6. Test Specimen Preparation**

For all testing scenarios, test decks were prepared as described above. Tile arrays consisted of six courses, five tiles wide each. Two Quik Drive #8 x 2.5 in WSCT Series Tile Roofing Screws (ASTM A641 Class 1) were used for mechanical attachment of concrete and model tiles. Polyfoam Products Inc. AH160 Two-Component Polyurethane Foam Roof Tile Adhesive (Polyset) was used for foam adhesive configurations. All adhesive set tiles were installed by registered technicians.

Three concrete tile arrays were installed (high/med/low profile) using foam adhesive. Prior to installation, polyethylene plastic sheeting was placed between the deck and foam adhesive in the fifth and sixth courses. This configuration allowed the tiles in those courses to be removed from the deck while still retaining the foam adhesive bonds to the tiles. This enabled the center tile in the fifth course to be replaced with the appropriate model tile. Additional plastic sheeting was also placed between the surface of the tile and the foam adhesive of the center tile in the fifth course. The result of this arrangement is a removable foam patty formed to the profile of the tile. High strength two-sided adhesive tape was used to bond each foam patty mold to the

appropriate model.

The (simulated) foam adhesive set model tile was then installed either alone on the deck (Phase I) or within an array (Phase I) using #8 x 2.5 in galvanized screws. The remaining (removable) foam adhesive set tiles from the fifth and sixth courses were also fastened mechanically for Phase II arrangements. This configuration enabled the wind flow characteristics around the model tile created by the foam adhesive, while still providing a secure attachment of the model and the surrounding tiles. All mechanical fastening locations were downwind of the pressure taps on the model tile, thus the mechanical fasteners were assumed to have a negligible impact on wind flow conditions.

**Phase I Specimens.** Phase I specimens consisted of a single model tile attached to the test deck turntable. Two #8 x 2.5 in galvanized screws were used for attachment of mechanically fastened specimens. Wind loading was applied for 2 min at three velocity levels (20, 30, and 40 m/s) at each of the five wind angles of attack, 0° (perpendicular to the leading edge), 22.5°, 45°, 67.5° and 90° (parallel to the leading edge). Table 1 lists the variables. Surface pressures on the model were captured during each test. Figure 4 shows a schematic of the turntable used to rotate the specimen. Figure 5 contains a picture of the high profile model in a cornering wind condition.

Table 1. Phase I test matrix variables

Profile	Install Type (Isolated)	Wind Velocity	Wind Angle	Replicates
High	Mechanical Direct	20 m/s	0°	2
Medium	Mechanical w/ Battens	30 m/s	22.5°	
Low	Foam Adhesive Set	40 m/s	45°	
			67.5°	
			90°	

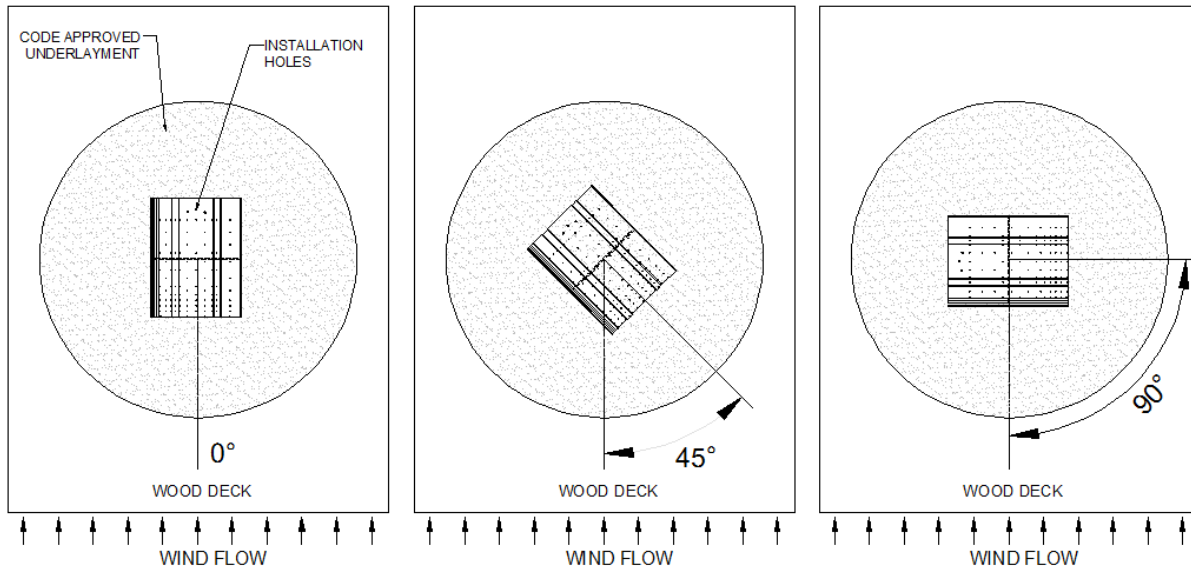


Figure 4. Turntable configuration used in Phase I testing



Figure 5. Mechanically fastened high profile model in Phase I configuration (45° wind angle)

**Phase II Specimens.** Phase II specimens incorporated a concrete tile array with a model tile installed in the center of the fifth course (see Figure 6). Trained technicians applied the foam adhesive. Tile arrays were installed such that wind loading was perpendicular to the leading edge (0°). Specimens were loaded for 2 min at 20, 30, and 40 m/s. Five replicates of each test were conducted. Table 2 lists the variables.

Table 2. Phase II test matrix variables

Profile	Install Type (Array)	Wind Velocity	Wind Angle	Replicates
High	Mechanical Direct	20 m/s	0°	5
Medium	Mechanical w/ Battens	30 m/s		
Low	Foam Adhesive Set	40 m/s		



Figure 6. Foam adhesive set medium profile array studied in Phase II testing

### 5.1.7. Results: Approach Flow Fields

**Isolated Tile Specimens.** The spatial variation in wind velocity was measured directly upwind of the Phase 1 specimen turntable. Three Cobra probes were mounted to a vertical rake attached to the center of the test deck. A fourth reference velocity Cobra probe was installed near the edge of the test deck at a height of 16 cm. The vertical rake probes captured three-axis wind velocities while reference wind speeds of 20, 30, and 40 m/s were generated across the test section. The rake was moved to new location and wind velocities were again captured at the rake for 20, 30, and 40 m/s reference wind speeds. This process was repeated at five locations laterally across the test deck at 10 cm increments. The Cobra probe mounting heights on the rake were then adjusted vertically and measurements were again taken at the five lateral locations across the deck. This arrangement was used to capture velocity measurement at each point on a 5 x 6 grid with 10 cm lateral resolution and 1.5 cm vertical resolution. The results of this process are displayed in Figure 7, which shows the two-dimensional spatial variation in wind approaching the model tile specimen, normalized by velocity measurements taken at the center of the test section and 10 cm above the deck. Absent the slight variation at 30 cm, the approach flow is uniform laterally across the test section. Wind velocity increases above heights 3 cm above the deck, which is expected. Boundary layers form immediately on the test section surfaces after the air leaves the setting chamber. All else being equal, higher profile tiles should be subjected to higher wind speeds. Surface pressure data for Phase I testing are not presented herein.

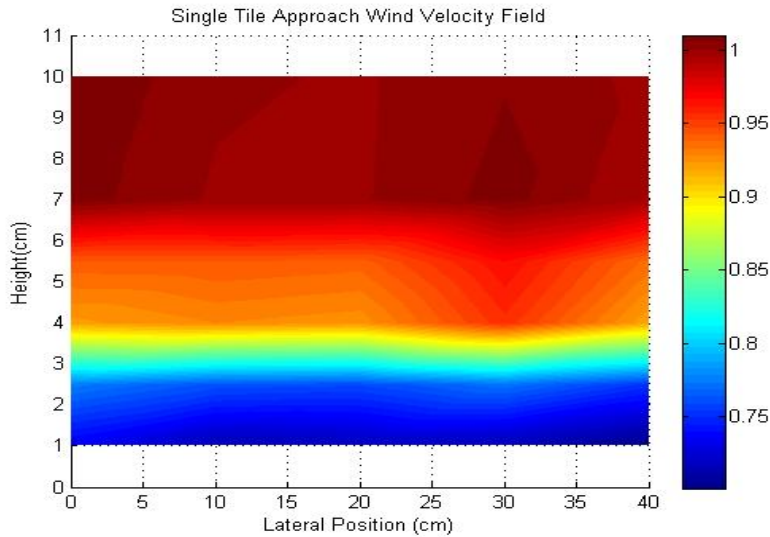


Figure 7. The approach wind velocity field normalized by reference velocity for the isolated tile

**Tile Array Specimens.** The spatial variation in wind velocity was measured for each of the three foam adhesive set tile arrays (high/medium/low profile) to assess the blockage effect of upwind tiles to the wind load imparted on the model tile. In order to capture the spatial variation in approach flow, three Cobra probes were mounted to a horizontal rake (see Figure 8) at 5 cm (2 in) in front of the model tile and 1 cm above the tile in the course below the model tile. A reference Cobra probe adjusted to a height of 16 cm above the test deck and located 10 cm (4 in) from the leading edge of the test deck and 10 cm (4 in) from side of the test deck, so as not to disrupt wind flow approaching the model tile, was also used to record velocity and static pressure data for all wind load scenarios. Velocity and static pressure measurements were taken at the rake for reference wind speeds of 20, 30, and 40 m/s. The rake was then raised 1 cm and measurements repeated at the three reference wind speeds. This process was repeated in 1 cm increments until measurements were taken at a height of 9 cm above the tile in the course below the model tile. The Cobra probes were then adjusted to three new horizontal positions and the rake was again lowered to a 1 cm height. This process of vertical and horizontal Cobra probe positioning and measurement was repeated until nine vertical (1 cm resolution) wind speed and static pressure measurements were taken at nine lateral points across the leading edge of the tile. After approach flow measurements were taken for each foam adhesive array, the Cobra probe rake was removed, leaving only the reference Cobra probe inside the test section. All testing subsequent testing for Phase II was conducted using a single probe at the reference location.



Figure 8. Cobra probe rake positioned above the medium profile roofing tile array

The resultant spatial variations in approach velocity for each tile profile are shown in Figure 9. The high profile tile experiences significantly high wind speeds on the higher interlocking side. The medium profile tile exhibits less extreme, but similar, behavior with regard to higher approach wind speeds on the interlocking side. The low profile tile also experiences higher wind speed very near the interlocking edge but also experiences relatively lower wind speeds moving toward the center away from the interlocking edge. The variation in approach wind speed for low profile tiles is surprising considering the absence of profile to interact with wind upstream of the model tile.

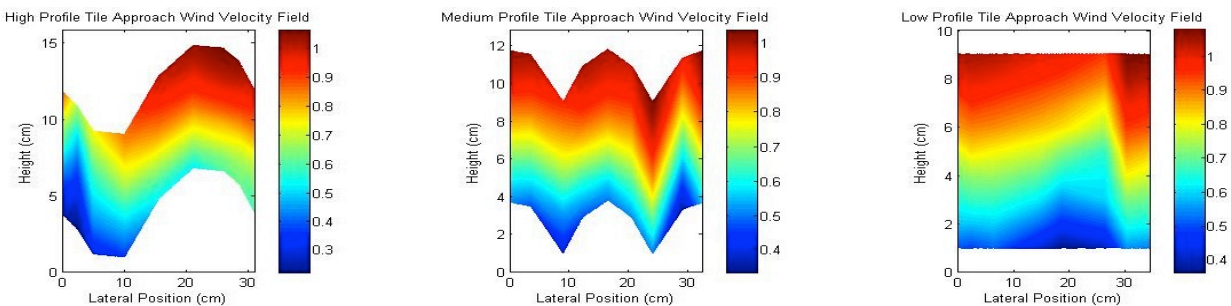


Figure 9. High, medium, and low profile tile approach wind velocity fields normalized by reference velocity

### 5.1.8. Results: Surface Pressure Distribution

TAS 108-95 provides specification of the procedure for estimating the lift coefficient ( $C_L$ ) for a roofing tile. The lift coefficient is used in Equation 16-33 of the 2010 Florida Building Code to estimate design wind loads for roof tiles. The methodology presented in TAS 108-95 for measuring surface pressures on roofing tiles and estimating wind load parameters is based on the assumption that wind induced surface pressures are uniform in the lateral direction across the tile. In accordance with this assumption TAS 108-95 requires 20 pressure taps along the centerline of the upper surface and seven pressure taps along the centerline of the bottom surface of the tile to be analyzed. In order to evaluate the validity of this assumption, surface pressures were captured on model tiles with 256 pressure taps distributed across the entire areas of the upper and lower surfaces. The mean surface pressure at each tap is converted to a dimensionless pressure coefficient using the following equation:

$$C_p = \frac{P - P_\infty}{q} \quad (6)$$

where  $C_p$  = coefficient of pressure,  $P$  = mean local pressure on component,  $P_\infty$  = mean free stream static pressure,  $q$  = mean velocity pressure

Figure 10 shows the spatial distribution of  $C_p$  values for the upper surface, lower surface, and net area respectively (from left to right) of a high profile model tile installed mechanically direct to deck within an array (Phase II specimen) and subjected to wind load inside the test section of the DFS. The wind angle of attack was perpendicular to the leading edge of the tile (right to left in Figure 10). The  $C_p$  distribution across the tile upper surface is uniform in the lateral direction. The lateral distribution on the lower surface fluctuates near the leading edge, however, the small magnitude of these fluctuations relative to the  $C_p$  values on the upper surface yield a net distribution that is uniform in the lateral direction. The implication of this result is that the lateral uniformity of surface pressure, assumed by the methodology presented by TAS 108-95 is valid for a  $0^\circ$  wind angle of attack.

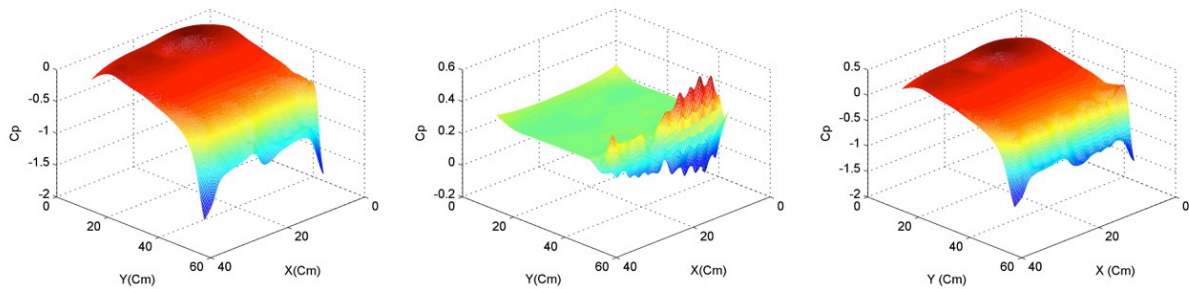


Figure 10. Upper surface, lower surface, and net spatial  $C_p$  distributions for high profile tile array with mechanical direct to deck installation

In order to verify this finding numerically, lift coefficients ( $C_L$ ) for each tile array specimen were calculated using two different methods. The first method is intended to represent the lift coefficient as calculated using TAS 108-95.

$$C_L = \frac{\sum C_{pb} \delta_b}{l * b} - \frac{\sum C_{tb} \delta_t}{l * b} \quad (7)$$

where  $C_{pb}$  = pressure coefficient on the bottom surface of the tile,  $\delta_b$  = tributary area of corresponding bottom surface pressure coefficient,  $C_{pt}$  = pressure coefficient on the top surface of the tile,  $\delta_t$  = tributary area of corresponding top surface pressure coefficient,  $l$  = length of the tile, and  $b$  = exposed width of the tile.

The physical location of pressure taps on model tiles do not correspond to the exact locations along the centerline of the tile as specified by TAS 108-85. To overcome this issue, the surface pressures at locations specified by TAS 108-95 were interpolated using all pressure taps on the model. This validity of this estimation method is assumed reasonable considering the lateral uniformity of surface pressures.

The second method for estimating the lift coefficients incorporates the pressures captured by all taps on the upper and lower surfaces of the models. The modified lift coefficient ( $C'_L$ ) is calculated by as described by Eq. 3.

$$C'_L = \frac{\sum C'_{pt} \delta \cos(\varphi) \cos(\theta)}{l * b} - \frac{\sum C'_{pb} \delta \cos(\theta) \cos(\varphi)}{l * b} \quad (8)$$

where  $C'_{pb}$  = 4-node average pressure coefficient on the bottom surface of the tile,  $\delta$  = tributary area of corresponding 4-node average pressure coefficient,  $C'_{pt}$  = 4-node average pressure coefficient on the top surface of the tile,  $l$  = length of the tile, and  $b$  = exposed width of the tile,  $\theta$  = the slope ( $dz/dx$ ) in the direction parallel to the leading edge of the roof tile at the location of the 4-node average pressure coefficient,  $\varphi$  = the slope ( $dz/dy$ ) in the direction perpendicular to the leading edge of the roof tile at the location of the 4-node average pressure coefficient.

The resultant calculation of the lift coefficient (TAS 108-95) and the modified lift coefficient for each tile array specimen are presented in Figure 11. In all cases the values for each lift coefficient are similar. The implication of these results is that the TAS 108-95 methodology of estimating lift coefficient based on using pressure taps along the centerline and assuming lateral uniformity of surface pressures is a valid for the case where the wind is traveling head on the roofing tile. A lift coefficient of 0.2 is permitted for use with Equation 16-33 of the Florida Building Code as a substitute for calculating lift coefficients as per TAS 108-95. The majority of lift coefficients resulting from this experiment were greater than 0.2, which suggests that the use of 0.2 for design may not be conservative.

The DFS did not become available for regular use until late spring, and therefore it was not possible to evaluate other wind directions. We believe this to be a critical issue that warrants additional study as soon as possible.

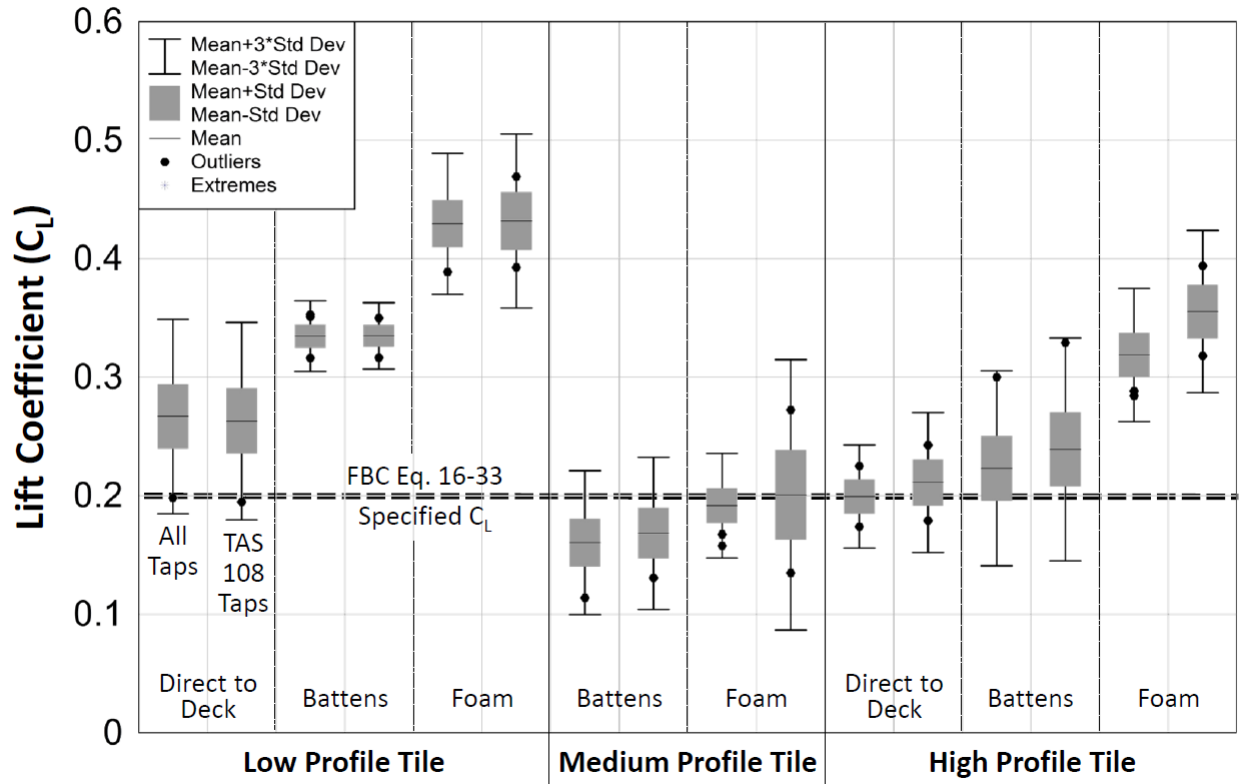


Figure 11. Comparison of lift coefficient values to specified values in the Florida Building Code

## 5.2. Attachment Forces Restraining Field Roofing Tiles

### 5.2.1. Experimental Configuration

Concrete field roofing tiles affixed to the load cells at the attachment location were subjected to wind loading. The DFS was used to generate near roof surface wind conditions over a partial mockup of a tile roof system. The attachment configuration for all tile arrays included a single Quik Drive #8 x 2.5 in WSCT Series Tile Roofing Screw (ASTM A641 Class 1) installed in the left installation hole (looking at the leading edge of the tile). The concrete tile located in the center of the fifth course was installed using a single #8 machine screw designed for compatibility with the load cell arrangement. The load cell arrangement was installed below the deck such that the fastening location for the #8 machine screw was level with the deck. The list of variables is shown in Table 3.

Table 3. Test matrix variables

Profile	Install Type (Array)	Wind Velocity	Wind Angle	Replicates
High	Mech. (1 #8 Screw) Direct	20 m/s	0°	5
Medium	Mech. (1 #8 Screw) w/ Battens	30 m/s		
Low		40 m/s		

### 5.2.2. Testing Apparatus

The DFS was used to simulate near roof wind conditions as described in Section 4.1.1.2.

### 5.2.3. Load Cell Measurement System

A single six-axis load cell was used to measure wind forces on the roof tile mechanical fasteners (Figure 12). The load cells are capable of resolving forces and moments in the X-, Y-, and Z-planes. Six-axis load cells are required, as opposed to single/three-axis load cells, because the attachment of the load cells to the Instrument Tile fastening is an eccentric connection. This eccentricity will cause in-plane forces on the tile to be read as moments by the load cell. Without the ability to isolate the forces from the moments, the in-plane forces measurements would lose accuracy.

One ATI Industrial Automation model Nano25 (IP65) six-axis load cell was placed below the tile fastener as shown in Figure 12. The load cell consists of a 28 mm (1.1 in) diameter by 28 mm (1.1 in) tall steel cylinder with silicon strain gauges fixed on the interior face. The sensing ranges and resolutions for the load axis are given in Table 4. The load readings were captured via National Instruments Labview 2010 and a DAQ analog-to-digital converter.

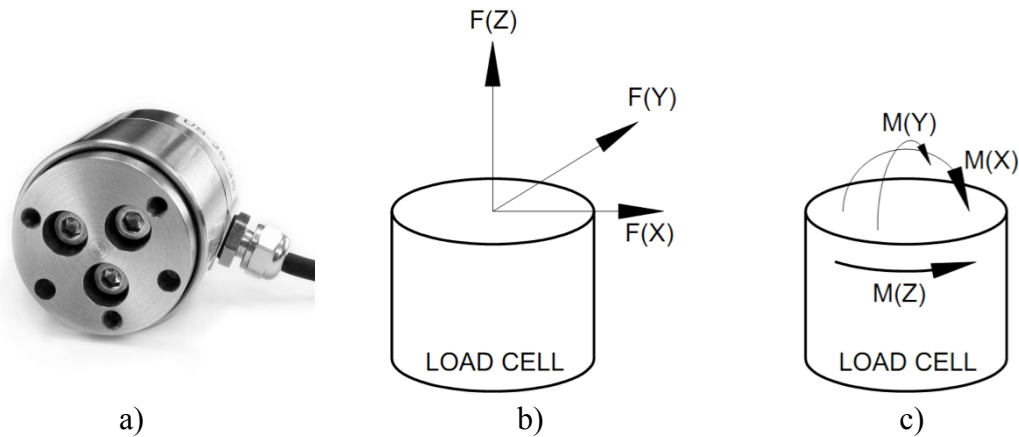


Figure 12. Six-axis load cell and measured forces/moments

Table 4. Six-axis load cell sensing ranges and resolutions

Measurement Axis (see Figure 2)	F(X) N (lbf)	F(Y) N (lbf)	F(Z) N (lbf)	M(X) N-m (lbf-in)	M(Y) N-m (lbf-in)	M(Z) N-m (lbf-in)
Sensing Range	111.2 (25)	111.2 (25)	445 (100)	2.8 (25)	2.8 (25)	2.8 (25)
Sensing Resolution	1/50 (1/224)	1/50 (1/224)	3/50 (3/224)	1/1340 (1/160)	1/1340 (1/160)	1/2680 (1/320)

### 5.2.4. Velocity Measurement System

TFI Cobra Probes were used to capture the three-axis wind velocity within the test chamber. The specifications of the probes are as described in Section 4.1.1.4. A single Cobra probe was used to

record velocity and static pressure data 16 cm (6.3 in) above the test deck at a location 10 cm (4 in) from the leading edge of the test deck and 10 cm (4 in) from side of the test deck to avoid disrupting the approach flow.

### 5.2.5. Test Deck Preparation

Section 5.1.5 describes the composition of the test decks.

### 5.2.6. Instrumented Roofing Tiles

A single concrete tile within an array for each of the specimen configurations was instrumented with a six-axis load cell below its fastening. Figure 13 contains a schematic of a low profile tile instrumented for testing. The wood decking area below the fastener or foam is cut out and replaced with a load cell. A steel plate with a #8 size machined screw hole was used to transfer the load from fastener to load cell for measurement. A #8 x 2.5 in machine screw was used for attachment of the tile to the steel flat bar.

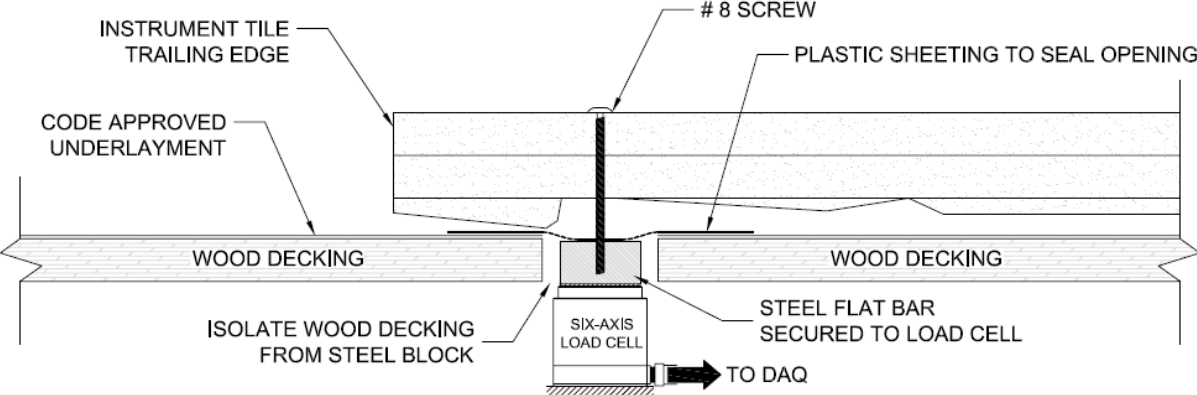


Figure 13. Side view of the load cell arrangement



Figure 14. Medium profile load cell arrangement

### 5.2.7. Results

The forces and moments measured by the six-axis load cells during testing are presented in the figures below. The modified lift coefficients ( $C'_L$ ) presented in a previous section were used to estimate the uplift moment at the tile fastening location as a function of wind speed. The restoring moments at the fastening due to the self-weight of the tiles were also calculated. Until the wind speed is high enough to create an uplift moment greater than the restoring moment, the forces and moments at the fastening locations are expected to be minimal. The vertical line on each of the plots below represents the point at which the predicted uplift moment exceeds the restoring moment of the tile. The uplift force on the fastener,  $F_z$ , most clearly suggests that once the uplift moment exceeds the restoring moments, the tile may be experiencing tail deflection (uplift) causing loading on the fastener to increase significantly. The results indicate there is a need for additional experimentation to determine the effect of roofing tile tail deflection on fastener loads.

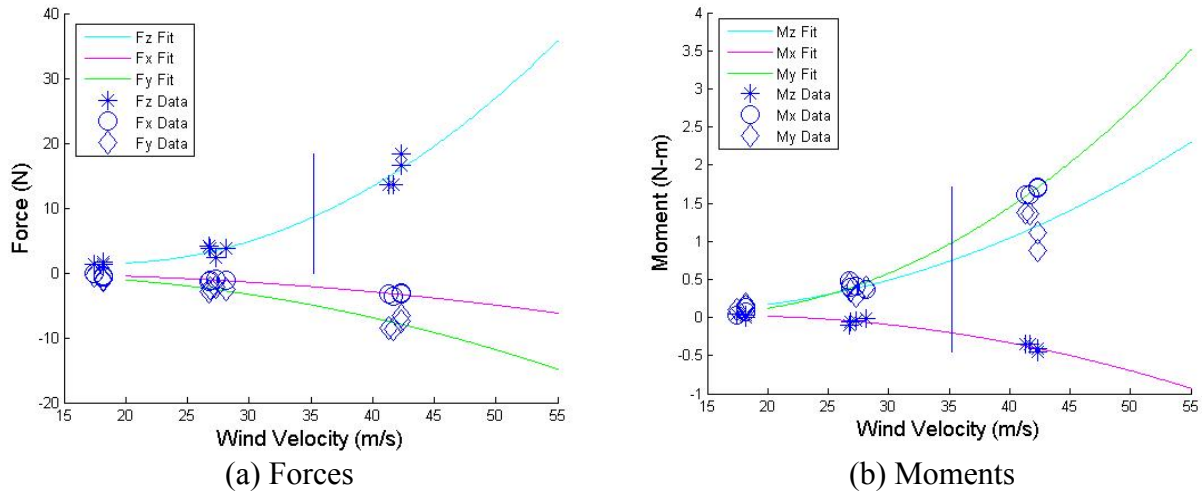


Figure 15. Measured attachment forces (left pane) and moments (right pane) for the low profile roofing tile as a function of wind speed

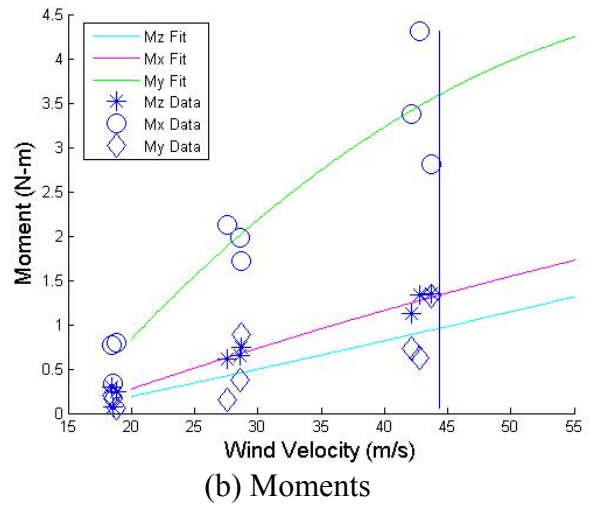
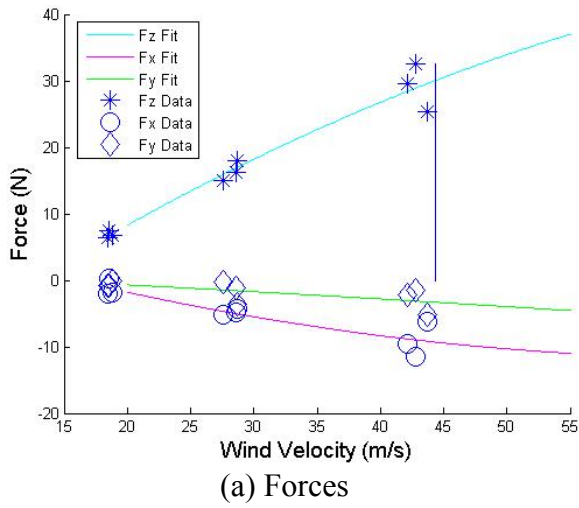


Figure 16. Measured attachment forces (left pane) and moments (right pane) for the medium-profile roofing tile with battens as a function of wind speed

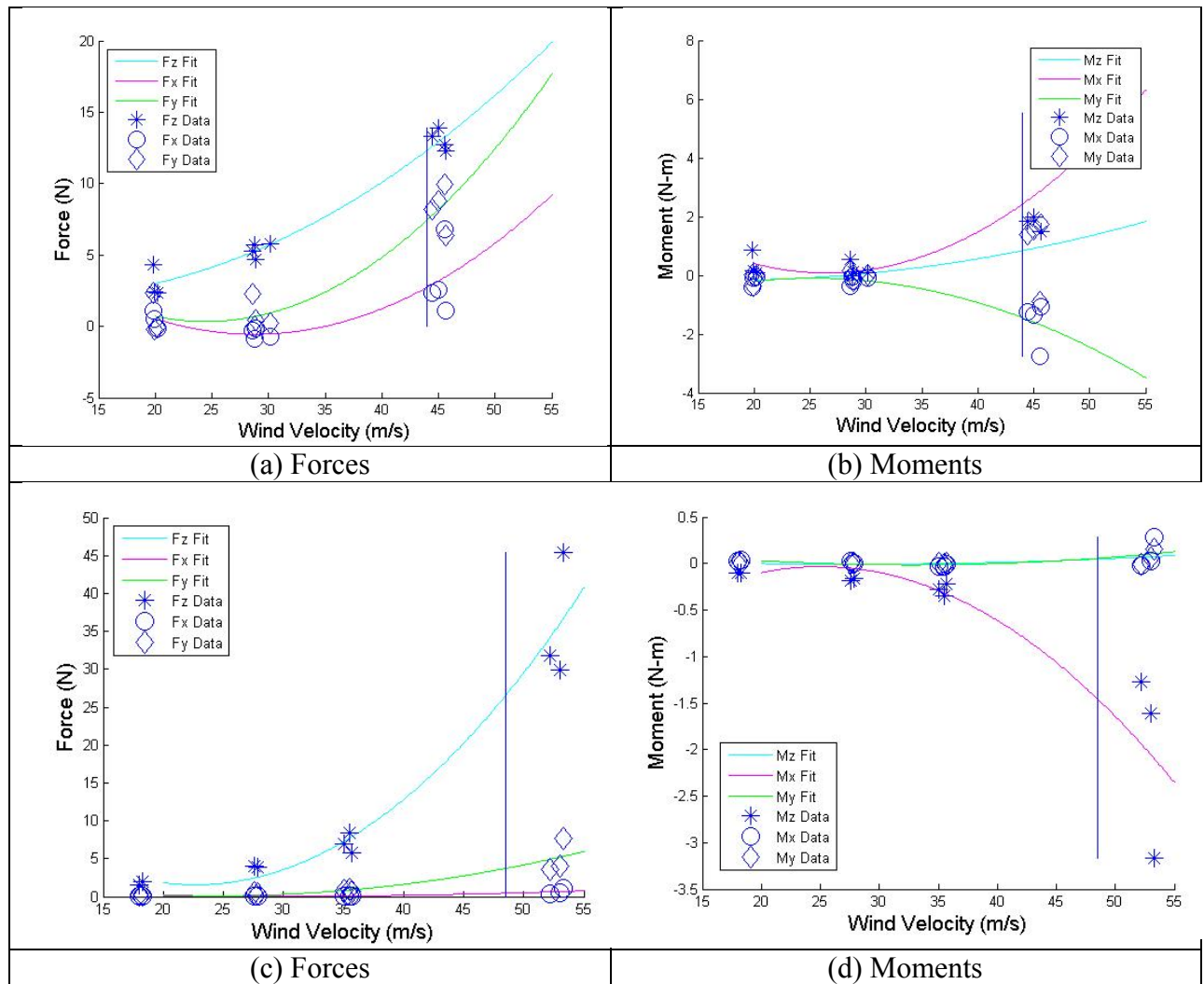


Figure 17. Measured attachment forces (left panes) and moments (right panes) for the high-profile roofing tile installed with battens (upper panes) and direct to deck (lower panes) as a function of wind speed

### 5.3. Mechanical Resistance of Roof Attachments

#### 5.3.1. Experimental Configuration

Concrete roof tiles were loaded at varied points along the tile centerline using concrete anchors and a dual column tabletop universal testing machine. Specimens included high, medium, and low profile tiles installed on plywood test decks using a single #8 x 2.5 in tile roofing screw. Direct to deck and batten configurations were examined. Five different points of load application were considered for each tile installation configuration by varying the location of the concrete anchor installation. Table 5 lists the variables.

Table 5. Test Matrix Variables

Profile	Install Type (Array)	Pull Locations	Replicates
High	Mech. (1 #8 Screw) Direct	5	10
Medium	Mech. (1 #8 Screw) w/ Battens		
Low			

### 5.3.2. Testing Apparatus

The testing apparatus consisted of an Instron Universal Testing Machine Model 3367 (UTM) and rigid steel frame designed to quickly change out specimens (Figure 18). The UTM has a 30 kN (6750 lbf) load capacity, with rated accuracy of  $\pm 0.5\%$  of the indicated load. The system incorporates Bluehill 2 software that allows 100 Hz sampling frequency. Load was transferred to tiles using a steel chain (assumed to be a rigid link), a steel jig, and concrete anchor installed at one of five locations along the centerline of the tile. The rigid steel frame was constructed using 50.8 mm (2 in) square steel tubing. The top of the frame has an incline of  $18.5^\circ$  (4:12). A pulley mounted to the UTM, enables the steel chain to be oriented such that loading is in the upward direction normal to the surface of each tile. A steel jig attached to the end of the steel chain was used for connection to the concrete anchor installed on each tile specimen.



Figure 18. Mechanical uplift testing apparatus and testing arrangement

### 5.3.3. Specimen Preparation

Test deck sheathing consisted of 38 cm (15 in) by 244 cm (8 ft) 15/32 performance category APA rated plywood with 32/16 span rating, and exposure 1 bond classification. A single Quik

Drive #8 x 2.5 in WSCT Series Tile Roofing Screw (ASTM A641 Class 1) was used for mechanical attachment of each specimen tile. Six tile specimens were installed on each 38.1 cm (15 in) by 2.4 m (8 ft) section of plywood. Concrete anchors were installed at one of five points along the centerline located at 8, 16, 24, 32, and 40 cm respectively from the head of each tile. Ten replicates of each combination of tile installation configuration and pull location were tested. The last tile, or “dummy tile”, on each test deck is present for proper orientation of the tiles above and was not subjected to loading. Head laps were 76.2 mm (3 in). A 25.4 mm (1 in) by 50.8 mm (2 in) by 38 cm (15 in) section of lumber was positioned below the lateral interlocking edge of high profile tiles during installation to simulate the effect of an adjacent tile. Battens were 25.4 mm (1 in) by 50.8 mm (2 in) by 38.1 cm (15 in) lumber installed using #8 x 2.5 in galvanized screws.

#### **5.3.4. Experimental Procedure**

A single, pre-constructed test deck was fixed to the rigid steel frame using rigid steel clamps fastened to the testing frame. The position of the test deck was such that the tile specimen in the highest course was loaded first. The UTM applied the load to the anchor of the specimen tile at 50.8 mm/min (2 in/min) using the steel loading chain. The swivel joint system is arranged to ensure that load is applied in the upward direction normal to the surface of the tile. Upward deflection of the specimen tile was measured by hand during load application.

Redland Technology proposed three considerations to govern the choice of failure criteria for uplift testing of mechanically attached roof tiles:

1. Ultimate failure of the fixing or tile
2. Excessive deflection, resulting in increased loading
3. A permanent set in the fixing which prevents the tile re-seating when the load is removed

The failure threshold for this experiment will correspond to ultimate failure or 50.8 mm (2 in) tail deflection for mechanical fastening.

After the specimen tile has reached the failure threshold, the loading jig is disconnected from the anchor and the tile is removed from the test deck. The clamps were released while the test deck was moved into position for load application to the next tile specimen. In this manner, five tiles on each test deck were loaded until failure, before the entire test deck was removed and replaced with the next deck.

#### **5.3.5. Results**

The methodology presented by TAS 102-95 estimates the attachment resistance of mechanically fastened roof tiles. The procedure for applying load to tile specimens attached to a mockup roof deck is intended to simulate the wind induced uplift forces acting on roof tiles. ERP 3 follows this methodology with regards to testing setup and experimental procedure with one exception. The angle of load application as specified by TAS 102-95 is in the vertical direction from the assumed aerodynamic center of the tile. As demonstrated in ERP 1, roof tiles subjected to wind load experience pressure on the upper and lower surfaces. Pressure acts normal to a surface, therefore the uplift forces induced on roof tiles from wind load must also act normal to the surface of the tile. This concept was the basis for applying load normal to the tile specimen surface in ERP 3. In order to compare the resistance values obtained from ERP 3 testing to product approval values calculated based on TAS 102-95, the vertical component of the uplift forces in ERP 3 were calculated using the angle of the tile relative to the deck and the magnitude

of the uplift force. The resolved vertical force is used to calculate attachment resistance ( $M_f$ ) using the following equations from TAS 102-95.

$$\bar{F} = \frac{1}{12} \sum_{i=1}^{12} F_i \quad (9)$$

where  $\bar{F}$  = average ultimate load (lbf),  $F$  = recorded ultimate load (lbf),  $i = 1, 2, 3, \dots, 12$  = test number. TAS 102-95 requires that 14 specimens for each configuration are tested, the highest and lowest resistance values are eliminated and analysis is conducted on the remaining 12. Ten specimens were tested for each configuration in ERP 3, highest and lowest values were eliminated and the remaining eight values are used for analysis in this section. TAS 102-95 requires the percent deviation from the mean ( $S'_F$ ) of each data set be lower than 20%. ERP 3 data was subject to the same requirement. The calculation is provided by the following two equations.

$$S_F = \sqrt{\frac{1}{12} \sum_{i=1}^{12} (F_i - \bar{F})^2} \quad (10)$$

where  $S_F$  = standard deviation,  $\bar{F}$  = average ultimate load (lbf),  $F$  = recorded ultimate load (lbf),  $i = 1, 2, 3, \dots, 12$  = test number

$$S'_F = \left( \frac{S_F}{\bar{F}} \right) \times 100 \quad (11)$$

where  $S'_F$  = percent deviation from the mean (%),  $S'_F$  = standard deviation,  $\bar{F}$  = average ultimate load (lbf)

$$F' = \left( \frac{\bar{F} - W}{MS} \right) \quad (12)$$

where  $F'$  = minimum characteristic resistance (lbf),  $\bar{F}$  = mean ultimate load (lbf),  $W$  = component's average weight (lbf) and  $MS$  = margin of safety = 2

$$M_f = [F' \times \cos(\theta - \alpha) \times L_f] \quad (13)$$

where  $M_f$  = attachment resistance (ft-lbf),  $F'$  = minimum characteristic resistance (lbf),  $\theta$  = test slope (degrees),  $\alpha$  = "test component angle" (degrees),  $L_f$  = tile's attachment moment arm (ft)

Table 6. Attachment Resistance Expressed as a Moment -  $M_f$  (ft-lbf)

Tile Profile	Fastener Type	Manufacturer		Measured	
		Direct Deck (min 15/32" plywood)	Battens	Direct Deck (min 15/32" plywood)	Battens
Product A (Low Profile)	1 #8 Screw	30.8	18.2	15.2	3.4
Product B (Medium Profile)	1 #8 Screw	25.8	22.9	17.9	6.0
Product C (High Profile)	1 #8 Screw	20.7	18.1	N/A	N/A

The high profile testing sets (battens and direct to deck) each exhibited percent deviations from the mean of greater than 20% and therefore were not included in calculations.

### 5.3.6. Conclusions

Table 6 compares product approval values for attachment resistance to resistance values calculated using the formulas above. The results clearly indicate that roof tile specimens as testing by ERP 3 underperformed with respect to attachment resistance. The key difference between the data sets is the angle of load application. When load is applied vertically to inclined tile specimens, a component of that load is in the in-plane direction (along the tile surface) creating shear reaction forces at the tile attachment. The other component of load is in the normal direction and is responsible for generation of moment at the fastening location. When uplift load is applied in the normal direction, as in ERP 3, the shear contribution is minimal, and the resultant moment at the fastening location is maximized. The clear discrepancy in attachment resistance values between ERP 3 and product approval may be due in part to this concept in conjunction with the fact that mechanical fasteners are in general more susceptible to moment forces than shear forces with regards to failure and withdrawal.

In addition to loading specimens at the assumed aerodynamic center (as prescribed by TAS 102-95), specimens were also loaded at four other points along the centerline of the tiles. The figures below represent the combination of applied moments and uplift at failure for each tile specimen loaded at Locations 1-5, which correspond to 8, 16, 24, 32, and 40 cm from the head of the tile. The applied uplift represents the load at which tile specimens failed, while the applied moment represents the failure load multiplied by the distance of the pull location from the axis of rotation of the tile specimen. The figures indicate that direct to deck installation configuration in general outperform their batten installation configuration counterparts. Moment resistance appears to be weakly dependent on uplift resistance for low profile specimens. Moment resistance seems to decrease with uplift force for medium profile specimens. High profile tiles exhibit the lowest resistance values of the three and seem to be consistent in general with regard to attachment resistances.

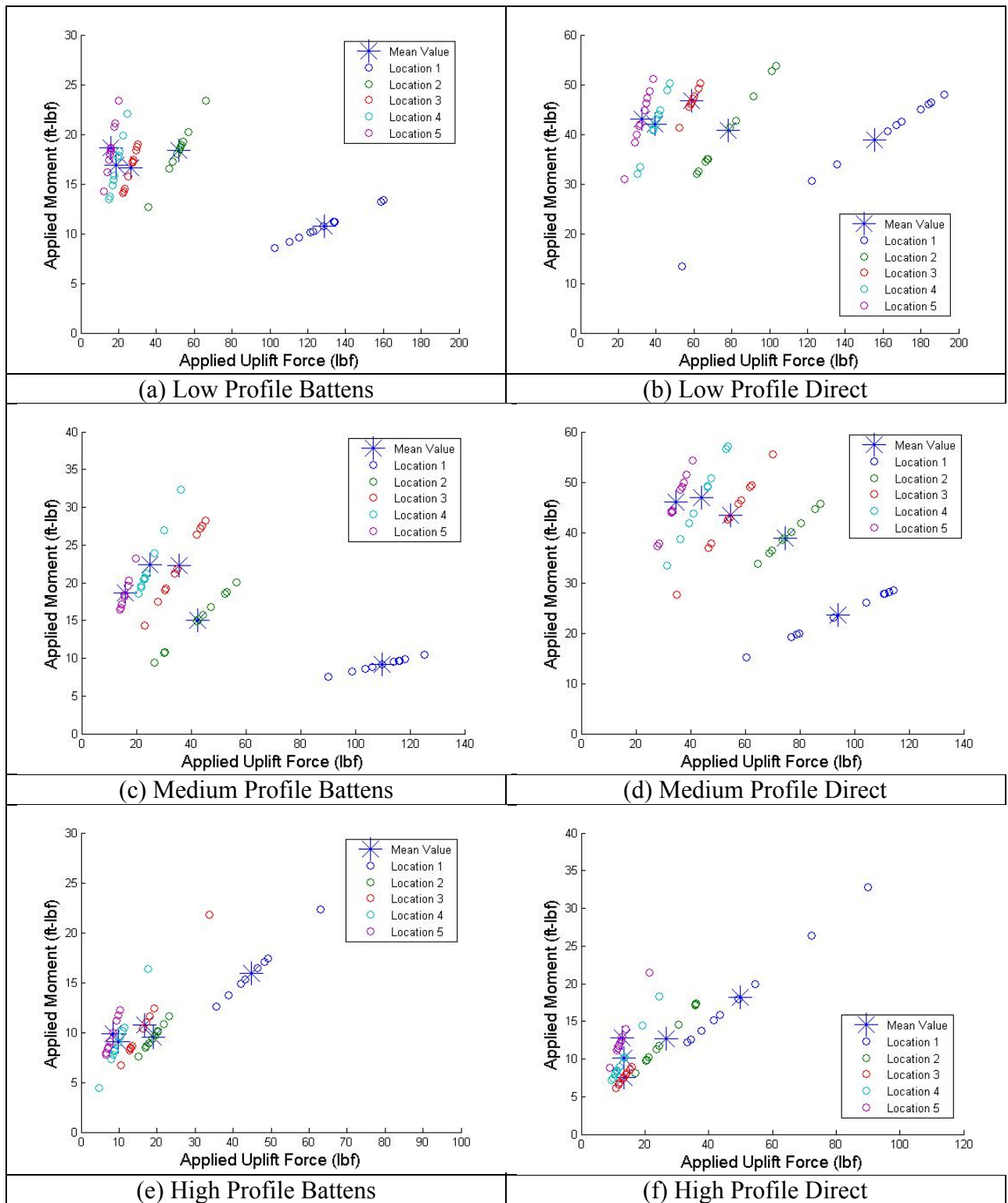


Figure 19. Moment-load diagrams for low- and medium-profile roofing tiles

**5.4. Wind Loading of Hip and Ridge Tiles**

A full-scale wind tunnel test was performed at Florida International University (FIU) to measure mean top and bottom surface pressures on high profile roofing tiles located in eave, rake, hip, and ridge roof conditions. Figure 20 shows a picture of the facility looking upwind. This section summarizes the experimental setup and preliminary results from surface pressure measurements on three ridge and six hip roofing tiles instrumented for the experiment. The Contractor coordinated with Dr. Arindam Chowdhury, who is leading up research for the Florida Division of Emergency Management directed at the performance of roofing tile systems. A preliminary analysis is provided below. The Contractor will be working with Dr. Chowdhury in the near term to develop a plan to synthesize the results of all experiments (UF and FIU).

**5.4.1. Testing Apparatus**

The WOW is an open return, subsonic wind tunnel facility. The system is a blower type, with 12 fans located at the intake section in a semi-circular arrangement. Each fan is powered by a 700-hp medium voltage electric motor, for a combined 8400-hp. The fans push air into a contraction chamber that increases the wind speed and produces uniform flow. The flow then travels through a set of triangular spires and floor roughness elements that generate turbulence and boundary layer characteristics before encountering the test building.



Figure 20. Florida International University Wall of Wind subsonic wind tunnel testing facility

The test matrix is shown below:

Table 7. Test matrix variables

Profile	Install Type (Array)	Wind Velocity	Wind Angles	Replicates
High	Mech. (2 #8 Screw) Direct	14 m/s (90°) 21 m/s (90°) 28 m/s (all angles)	0°, 30°, 45°, 60°, 90°, 120°, 135°, 150°, 180°	3 (at 90°) 1 (all other angles)

### 5.4.2. Test Building

As shown in Figure 21, the test building was a wood low-rise building with a foundation footprint of 2.7 m by 2.1 m (9 ft by 7 ft) and wall elevation of 2 m (6.5 ft). The roof was a half gable and half hip roof structure with a slope of four units vertical on twelve units horizontal, plan dimensions of 4 m by 3 m (13 ft by 10 ft), and a 0.6 m (2 ft) overhang beyond the structure's walls. The structural roof decking was 191 mm (0.625 in) thick wood sheathing with a hop mop base sheet installed over the decking. Mechanically fastened high profile roof tiles were installed over the base sheet with standard accessory tile pieces used for the rake, hip, and ridge conditions.

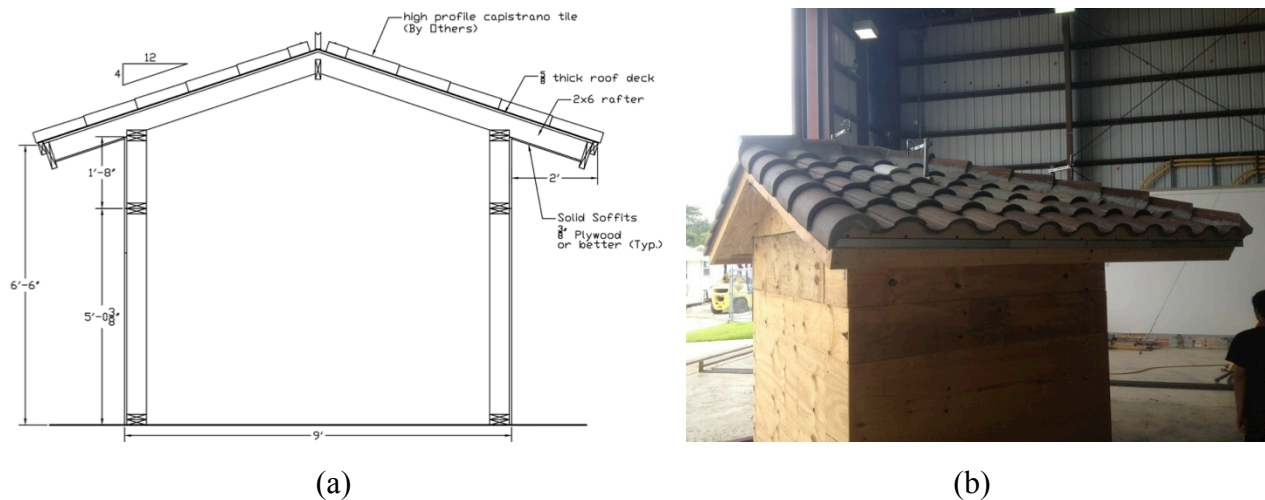


Figure 21. Test building (a) elevation plan and (b) as-built.

### 5.4.3. Instrumentation

The location of external surface pressure measurements on the eave, hip, and ridge tiles is shown in Figure 22. The focus of this section is the six hip (R1 through R6) and three ridge tiles (R7 through R8) instrumented for the experiment. Figure 3 shows a closer view of the tap locations on a single tile. For each tap location, the tile was drilled through the cross-section and tapped with a static pressure tube mounted flush with the top surface of the tile. The other side of the tube was connected to a Scanivalve pressure scanning system where pressures were measured relative to ambient pressure. Twenty taps were evenly distributed on the surface of the tile, producing an equivalent tributary area for all taps. Figure 23 presents the tile dimensions and tap layout.

For each instrumented tile, two taps were mounted below the tile to measure bottom surface pressure on the tile. One bottom surface tap was located on the centerline of the tile between the first (taps 1 through 5) and second (taps 6 through 10) rows, while the second

bottom surface tap was located on the centerline of the tile between the third (taps 11 through 15) and fourth (taps 16 through 20) rows. Approach wind flow was measured by a Turbulent Flow Instruments Cobra Probe (henceforth, Cobra Probe) located upstream of the test building at the mean roof height [2.6 m (8.5 ft)].

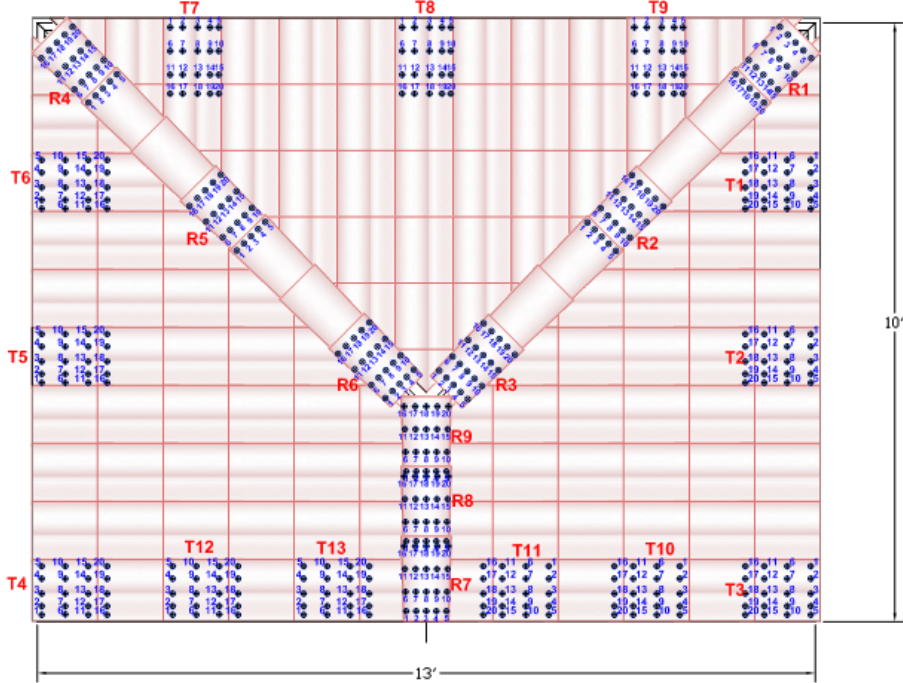


Figure 22. Roof plan with instrumented tiles on edge (T), ridge (R), and hip (H) roof conditions

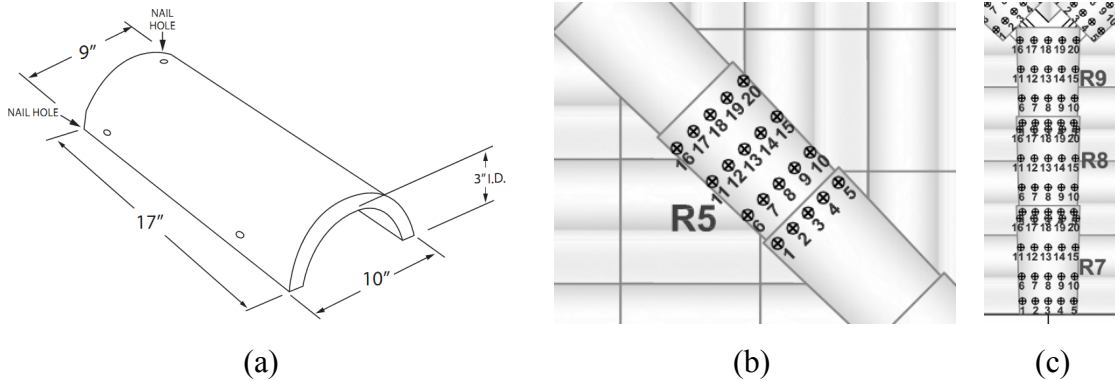


Figure 23. Hip and ridge tile (a) dimensions and location of top surface static pressure taps on (b) hip and (c) ridge tiles

**5.4.4. Testing Procedure**

The test building was mounted downwind of FIU’s Wall of Wind (WoW). The building was subjected to wind approaching the building at the nine different wind directions shown in Figure 24. For each 2 minute wind test, the building was immersed in a turbulent boundary layer wind

flow with a mean velocity profile corresponding to an open country exposure. A total of 17 tests were performed for this experiment and a summary of each test and corresponding wind direction and measured mean approach wind speed is given in Table 8. Pressure data on the tiles were captured along with the approach wind velocity for all tests. Test numbers 5 through 10 will not be discussed in this section due to the lower wind speeds.

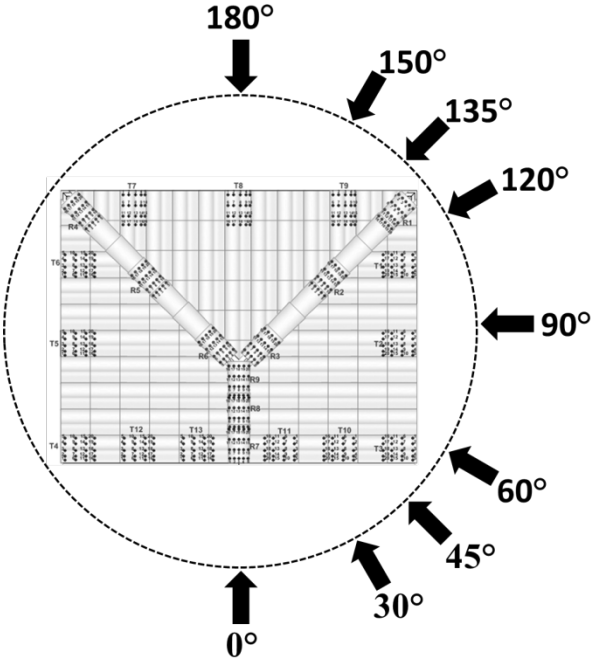


Figure 24. Wind directions

Table 8. Test number, wind direction, and corresponding mean approach wind speed.

Wind Test Number	Direction	Mean Approach Wind Speed (m/s)
1	0	27.7
2	30	27.8
3	45	27.9
4	60	27.9
5	90	13.9
6	90	13.9
7	90	13.9
8	90	20.9
9	90	20.9
10	90	20.9
11	90	27.9
12	90	28.0
13	90	27.8

14	120	28.0
15	135	28.1
16	150	28.1
17	180	27.9

#### 5.4.5. Preliminary Results

Mean tile surface pressure data were first computed for each tap, then normalized using Eq. 1 into a dimensionless pressure coefficient ( $C_p$ ) referenced to the mean approach wind velocity and static pressure measured by the Cobra Probe during the test.

$$C_p = \frac{P_{Ti} - P_{sa}}{\frac{1}{2} \rho V_a^2} \quad (14)$$

where  $P_{Ti}$  = mean pressure measured by the  $i$ th pressure tap on the tile,  $P_{sa}$  = mean static pressure measured by the Cobra Probe in the approach flow,  $\rho$  = air density, and  $V_a$  = mean approach velocity measured by the Cobra Probe at mean roof height. Surface contours were then generated for each hip and ridge tile to analyze the distribution of external surface pressure on the tile. An example of this output for each wind direction is shown in Figure 25 for hip tile R2 and Figure 26 for ridge tile R8. A negative coefficient of pressure ( $C_p$ ) represents an outward pressure vector normal to the tile surface and a positive  $C_p$  represents an inward pressure vector normal to the tile surface.

For hip tile R2, a negative  $C_p$  occurred over entirety of the tile for wind directions  $0^\circ$  through  $90^\circ$ . A leading edge flow separation is apparent for wind direction  $120^\circ$  through  $180^\circ$  with leeward  $C_p$  increasing with distance from the leading edge. The results indicate that for hip tile R2, flow parallel with the leading edge of the hip tile produces the lowest values of  $C_p$ , thus the external suction acting to lift the hip tile from the roof is greatest wind directions  $45^\circ$  through  $90^\circ$ . For ridge tile R8, negative  $C_p$  values were measured on all taps for all wind directions. Similar to hip tile R2, the lowest  $C_p$  values were measured on the  $45^\circ$  and  $60^\circ$  wind directions.

Lift coefficients, representing the dimensionless average net pressure acting on the tiles, were then developed for all instrumented hip and ridge tiles. The equation show in Eq. 2 to compute lift coefficient was adapted from TAS 108-95 for field tiles.

$$C_L = \frac{\sum C_{pb} \delta_b}{l * b} - \frac{\sum C_{tb} \delta_t}{l * b} \quad (15)$$

where  $C_{pb}$  = pressure coefficient on the bottom surface of the tile,  $\delta_b$  = tributary area of corresponding bottom surface pressure coefficient,  $C_{pt}$  = pressure coefficient on the top surface of the tile,  $\delta_t$  = tributary area of corresponding top surface pressure coefficient,  $l$  = length of the tile, and  $b$  = exposed width of the tile. The result of this analysis for all hip and ridge tiles is given in Figures 27 and 28.

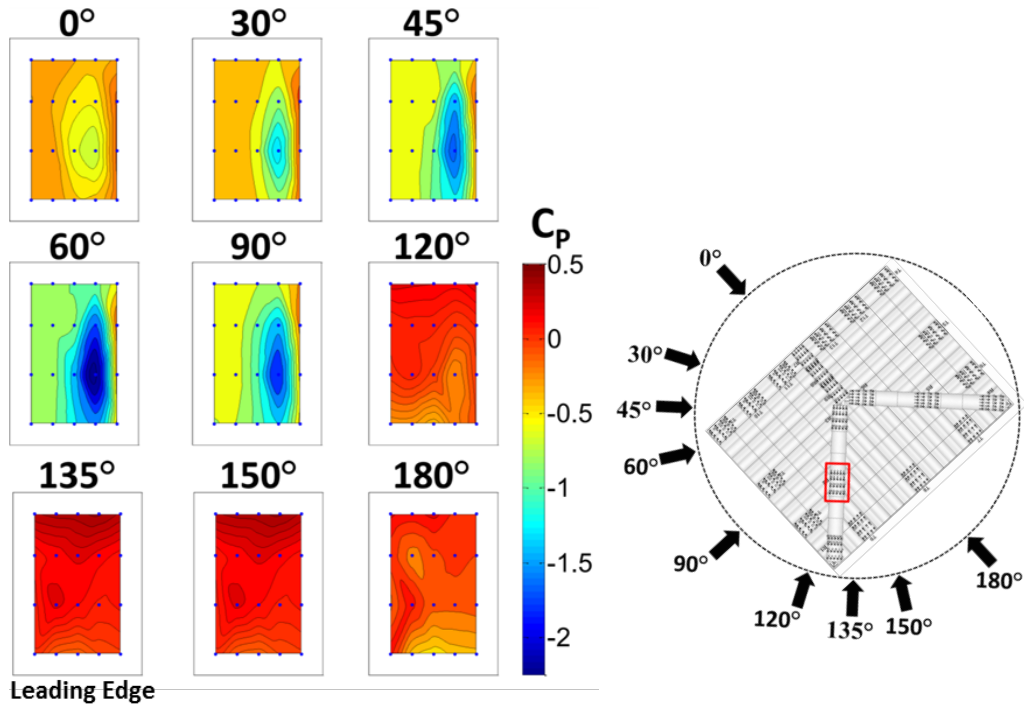


Figure 25. Contour plot of hip tile R2's mean external pressure coefficient normalized to mean approach flow conditions at mean roof height. The blue dots represent the location of surface pressure measurement.

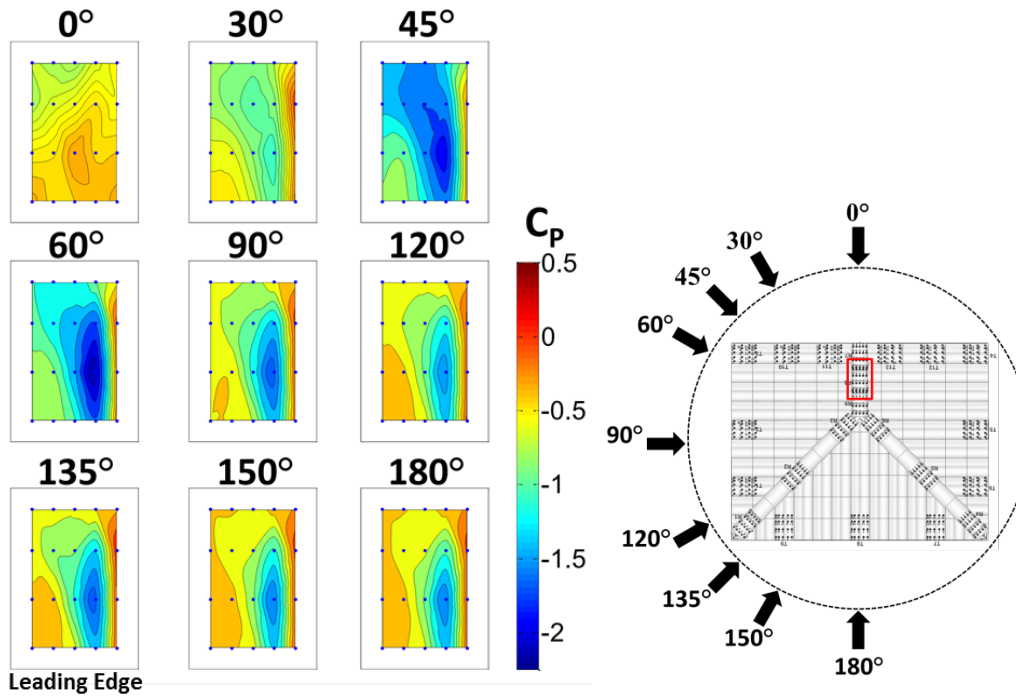


Figure 26. Contour plot of ridge tile R8's mean external pressure coefficient normalized to mean approach flow conditions at mean roof height. The blue dots represent the location of surface pressure measurement.

The similarity between lift coefficients for hip tiles on a single hip line is apparent in Figure 27. Tiles 1 through 3 reside on the same hip line and show that lift on the tile is greatest for wind parallel to their leading edge. This result matches findings from the pressure contour plot shown in Figure 25. Wind flow perpendicular to the leading edge produces the smallest values of lift on hip tiles. For ridge tiles, the lift coefficient results shown also indicate that wind direction is a leading factor in overall lift acting on the tile. The greatest amounts of lift on ridge tiles were generated for the 45° wind direction.

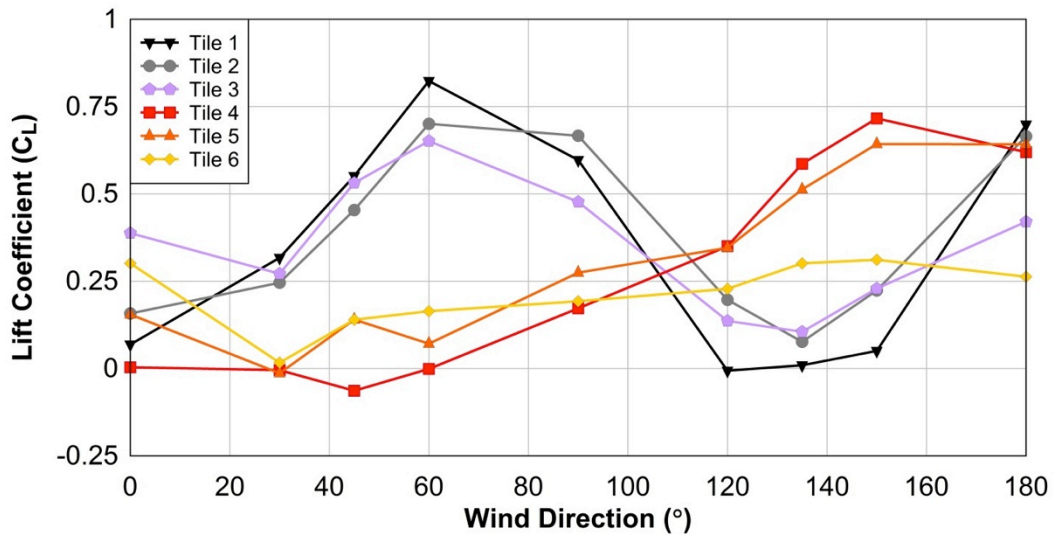


Figure 27. Hip tile lift coefficients referenced to the mean approach flow measured at mean roof height vs. wind direction.

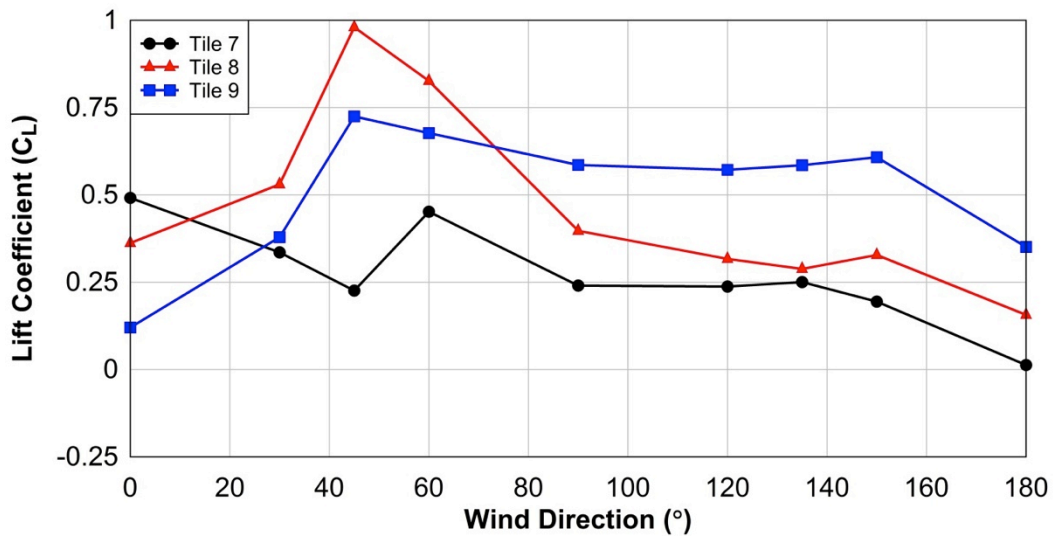


Figure 28. Ridge tile lift coefficients referenced to the mean approach flow measured at mean roof height vs. wind direction.

#### **5.4.6. Conclusions**

Wind pressures were measured on the upper and lower surfaces of hip and ridge tiles when immersed in wind from nine directions. The results of pressure distribution contours and lift coefficients indicate that the highest wind load on hip tiles occurs for wind flow directed parallel to the leading edge of the tile. The highest wind load on ridge tiles occurs for wind flow generated for the 45° wind direction. The 2010 Florida Building Code refers to FRSA 07320 for hip and ridge tile design pressures. FRSA 07320 presents conservative design pressures. However, details on the calculation procedure are absent. The results herein may be used to validate or develop standard methodologies for calculating hip and ridge tile design pressures.